# Oxygen Bubble Formation in a Glass Melt in the context of Nuclear Waste Vitrification

**Luiz Pereira, Annabelle Laplace**
CEA, DES, ISEC, DE2D, Univ Montpellier
Laboratoire de Développement des Matrices de Conditionnement
Marcoule – 30207 Bagnols-sur-Cèze, France
luiz.pereira@min.uni-muenchen.de, annabelle.laplace@cea.fr

**Franck Pigeonneau**
CEMEF, MINES ParisTech, PSL Research University, CNRS UMR7635
1 Claude Daunesse
06904, Sophia Antipolis Cedex, France
franck.pigeonneau@mines-paristech.fr

## ABSTRACT

This work takes place in the framework of nuclear waste vitrification and it deals with gas production occurring during the high-temperature process. We have focused on molecular oxygen ($O_2$) produced by redox reactions of multivalent elements. This phenomenon is also relevant to further natural and industrial systems. Our aim is to understand the mechanisms of oxygen bubble formation and growth, and how they are linked to redox reactions that occur during nuclear waste vitrification. We have performed different physico-chemical characterizations to support the understanding of bubble formation in the mentioned context. Experimental and numerical results of mass transfer between an isolated oxygen bubble and the melt, at varying content of the multivalent oxide (% $Ce_2O_3$) and varying oxygen fugacity ($fO_2$) are firstly presented. The results indicate that the presence of the multivalent element significantly enhances mass transfer from bubbles to melt, most acutely at reduced conditions and high contents. We further investigated a bubble population in a simplified nuclear waste glass melt. The melting of a granular starting glass, composed of glass beads, leads to a bubble population formed mainly due to air trapping. By assuming that the bubble dynamics is driven by their residence time in the crucible, the overall dynamics at various temperatures can be rationalized, scaled, and generalized.

## 1 INTRODUCTION

Nuclear waste vitrification is the current solution for nuclear waste containment in different countries. In France, this is the current measure taken for immobilizing both high-level waste (HLW) and some intermediate-level long-lived waste (ILW-LL). Indeed, by the early 1960's, glasses started to be considered as an option for immobilizing high-level waste solutions.[1] This vitrification process was firstly implemented at Saclay and later in Marcoule.[1]

Vitrification is not a simple encapsulation procedure. It consists in making a new material, in which the glass matrix is chemically bonded to the atoms from the nuclear waste. These atoms can then only be released by the destruction of the network bonds. Most of the countries dealing

with nuclear waste vitrification have adopted a borosilicate glass composition as hosting matrix.[2]

Several types of gases and possibly bubbles may be observed in vitrification processes of nuclear waste. Generally, one can highlight the formation of $NO_x$, $CO_2$, and $O_2$. This latter species is mainly produced by redox reaction of multivalent elements. Nuclear waste may contain different multivalent elements, such as cerium, iron, and chromium.[3] In molten oxide glasses, due to the great oxygen availability, $O_2^{diss}/O^{2-}$ redox couple is involved in redox reactions. Eq. 1 shows an example of redox reaction with cerium ($Ce^{4+}/Ce^{3+}$) in a molten oxide glass. As this equation progresses towards the right, molecular oxygen forms until it reaches the saturation of the glass melt. This saturation is characterized by the maximum amount of gas that can be dissolved at a given temperature and pressure. Thus, after overcoming this saturation threshold, the gas is energetically more stable as a gaseous phase than as a dissolved component, and, as a consequence, bubble formation occurs.

$$Ce^{4+} + \frac{1}{2} O^{2-} \rightleftarrows Ce^{3+} + \frac{1}{4} O_{2(g)}. \tag{1}$$
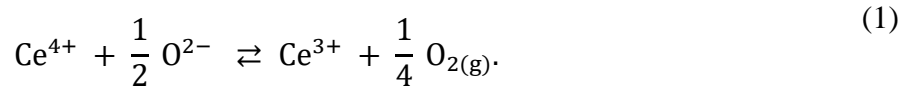
There is a great complexity in the chemistry of nuclear waste glasses. In order to be able to rationalize the results fundamentally, here, we simplified the system by choosing a borosilicate glass doped with cerium oxide (up to 1.5 wt%). This multivalent element was chosen due to its redox potential and its common presence in nuclear waste. Here, we present results on oxygen bubble formation in this simplified nuclear glass melt. Firstly, we describe essential physico-chemical characterizations of the system (carried out during PhD studies). Next, we present experimental and numerical results on the mass transfer in the presence of a single oxygen bubble immersed in a simplified nuclear melt ($T$ = 1150 °C), as a function of polyvalent element concentration (% $Ce_2O_3$) and oxygen fugacity ($fO_2$). Subsequently, we expand the system to a bubble population scenario and an investigation involving varying temperature ($T$) and duration ($t$). In this way, we present the general overview of the formation of bubbles; their evolution as a function of time, temperature and properties of the system; and their residence time in a simplified nuclear waste molten glass.

## 2    PHYSICO-CHEMICAL CHARACTERIZATION

In the framework of PhD work (Pereira 2020[4]), different physico-chemical characterizations were carried out to support the comprehension of oxygen bubble formation and to feed the computational simulations. The particle size distribution (PSD) of the borosilicate glass and the $CeO_2$ powders were obtained by laser granulometry technique. Using a coaxial cylinder viscosimeter coupled to a resistance furnace, viscosity measurements at high-temperature were done on the molten borosilicates. We obtained surface tension values between an oxygen bubble and the borosilicate melts for different temperatures (1000 – 1250 °C) using the maximum-bubble pressure method. Archimedean method was applied to reach the cerium-bearing borosilicate melt density, obtained at 1000 – 1300 °C.[4-6]

Besides these physical characterizations, chemical characterizations were also executed. Oxygen fugacity was measured using potentiometry technique, cerium speciation was obtained through XANES spectroscopy, and bubble gas analyses was evaluated using a mass spectrometer device coupled with a vacuum chamber. Figure 1 displays two examples of the mentioned results for surface tension and density at high-temperature.[5]
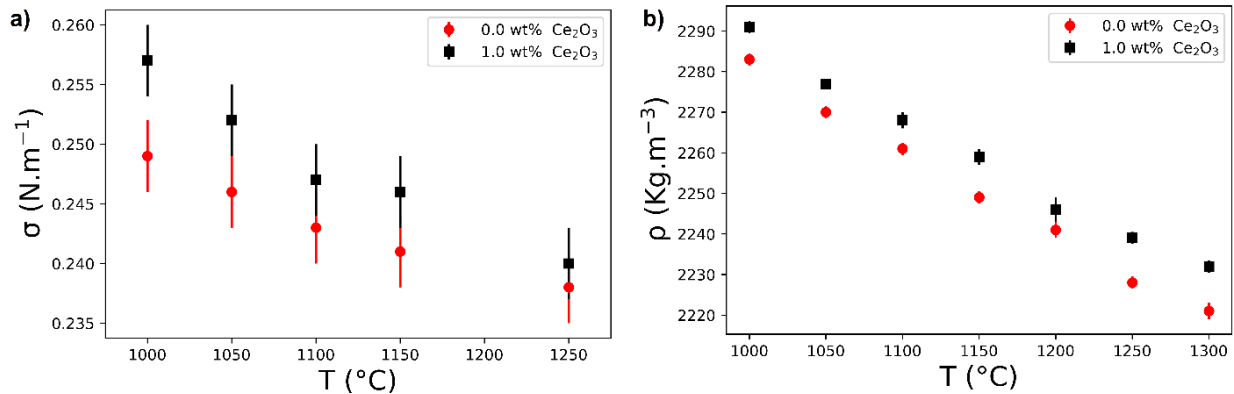
Figure 1: High-temperature results of a) surface tension between an oxygen bubble and the borosilicate melts with 0.0 and 1.0 wt% of $Ce_2O_3$.and b) density of borosilicate melts with 0.0 and 1.0 wt% of $Ce_2O_3$.

## 3    CASE 1: SINGLE BUBBLE

In this section, we describe how an isolated oxygen bubble immersed in a simplified nuclear waste glass melt behaves in terms of mass transfer as a function of multivalent content and oxygen fugacity. In our previous work (Pereira *et al.* 2020[5]), we studied the mass transfer between an oxygen rising bubble and a borosilicate melt doped with cerium oxide. This latter element has two possible valence states in silicate melts: $Ce^{4+}$/ $Ce^{3+}$.[3] Three cerium contents were used in this study (% $Ce_2O_3$ = 0.5, 1.0, and 1.5 wt%) as well as three different oxygen fugacities ($\log(fO_2$, atm) = 0, -0.7, -1.2). These different redox states are also called oxidized (O), intermediate (I), and reduced (R), respectively (9 molten glasses in total). In each of these scenarios, five bubbles were investigated leading to 45 different experiments.

High-temperature camera *in-situ* observation[7] was applied to understand the mass transfer between the rising oxygen bubble and the melt. This apparatus is a well-established technique employed to obtain information on glasses and melts at high temperatures. It consists of an electrical furnace coupled with a porthole, which geometrically links the glass melt sample to a charge-coupled device (CCD) camera. An oxygen bubble is artificially inflated in the melt and its evolution is recorded using this aforementioned device. The experimental part of this work was carried out in collaboration with Dr. Jaroslav Kloužek during my exchange program at the University of Chemistry and Technology, Prague (VŠCHT Praha) in 2020.

Numerical simulations[8] were also employed to study the mass transfer between a multicomponent bubble and the melt. In this model, the present gases dissolved gases are: $O_2$, $CO_2$, $N_2$[5]. It is a theoretical model considering the mass transfer phenomenon between a freely-rising bubble of a known initial composition with a molten glass with well-defined physico-chemical properties (discussed in section 2.0) and redox equilibrium (Eq. 1).

Figure 2, from Pereira *et al.* 2020[5], displays a bubble shrinking in a molten glass obtained from the aforementioned experimental approach as well as by two numerical models. The model A considers gases as independent entities not related to chemical reactions. Model B, on the other hand, takes into consideration cerium redox reaction, with involves molecular oxygen gas and enhance the mass transfer. As shown in Figure 2, the presence of the cerium oxide, even in small amounts (up to 1.5 wt%), enhances considerably the mass transfer. The model considering this latter situation (model B) is the one which describes well the acquired experimental data. This behavior was observed in all the experimental scenarios previously described.[5, 8]
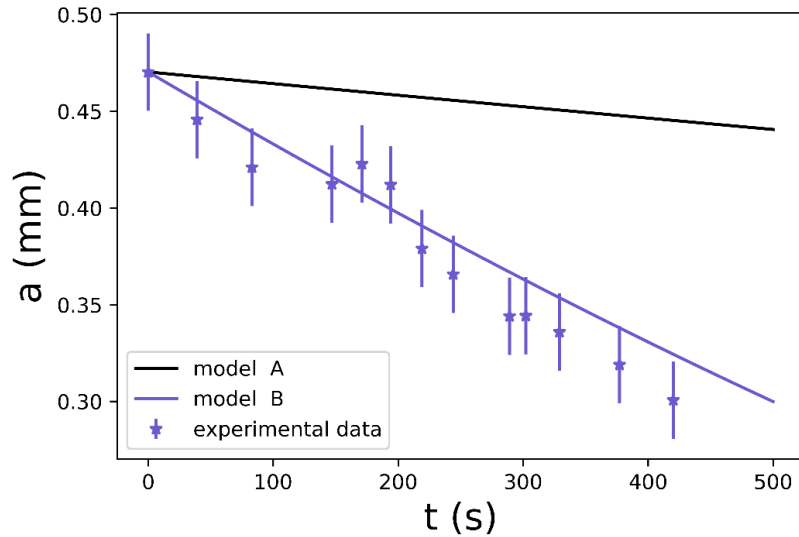
Figure 2: Bubble radius (a) as a function of time obtained experimentally and by two numerical models: A and B. The former does not consider redox reactions on the mass transfer calculations and the latter does.

All the bubble shrinkage experimental data from Pereira *et al.* 2020[5] were gathered and the experimental durations ($t$) were normalized by the characteristic time of mass transfer ($\tau$)[9], as displayed in Eq. 2.

$$\bar{t} = \frac{t}{\tau} = \frac{t\, 2a_0^2}{Sh_{O_2} D_{O_2} L_{O_2} RT}, \tag{2}$$

where $a_0^2$ is the initial bubble radius; $Sh_{O_2}$ is the Sherwood number, which is a function of the bubble characteristic (radius and composition) and chemical properties of the melt at the initial conditions; and the product $D_{O_2} L_{O_2} RT$ is the oxygen permeability. Therefore, by normalizing the experimental time by the characteristic time of mass transfer, we are considering not only the advection effect on mass transfer but also the effect of the redox reaction (amount of multivalent and oxygen fugacity).

It was also proposed a dimensionless shrinkage rate ($d\bar{a}/d\bar{t}$),[9] which is given by the Eq. 3:

$$\frac{d\bar{a}}{d\bar{t}} = -\frac{1}{\bar{a}} \sum_{i=1}^{N_g} \frac{\overline{Sh_i}}{\overline{\tau_i}} \left( x_i - Sa_{i,0} \right). \tag{3}$$

The bars over the variables indicate that they are dimensionless. The driving force for the bubble evolution over time is determined by the difference of the molar fraction ($x_i$) and the saturation state of the melt for each gaseous species ($Sa_{i,0}$). This dimensionless shrinkage rate is also a function of the Sherwood number and the saturation state of the melt, being therefore strongly dependent of the multivalent element and redox state of the melt. By solving this last equation, for short durations, the square root of the dimensionless radius ($\sqrt{\bar{a}}$) behaves as follows:

$$\sqrt{\bar{a}} = 1 - \beta\bar{t}. \tag{4}$$

Figure 3 assembles the experimental data from Pereira *et al.* 2020.[5] The square root of the dimensionless radius ($\sqrt{\bar{a}}$) is plotted as a function of the aforementioned normalized time ($\bar{t}$). A universal behavior appeared clearly for all redox states (O, I, R) and all cerium contents (0.5, 1.0, 1.5 wt%). It demonstrates how important is the bubble and melt characteristics, such as initial bubble radius and redox reaction of a multivalent element. The solid black line is a fitted curve, corresponding to Eq. 4 with β = 1.25. We concluded that mass transfer between a rising bubble and a molten silicate glass is enhanced in a presence of a multivalent element.[4, 5] More precisely, mass transfer in a simplified nuclear glass melt is increased at reduced conditions (low $f$O$_2$) and at high multivalent contents.
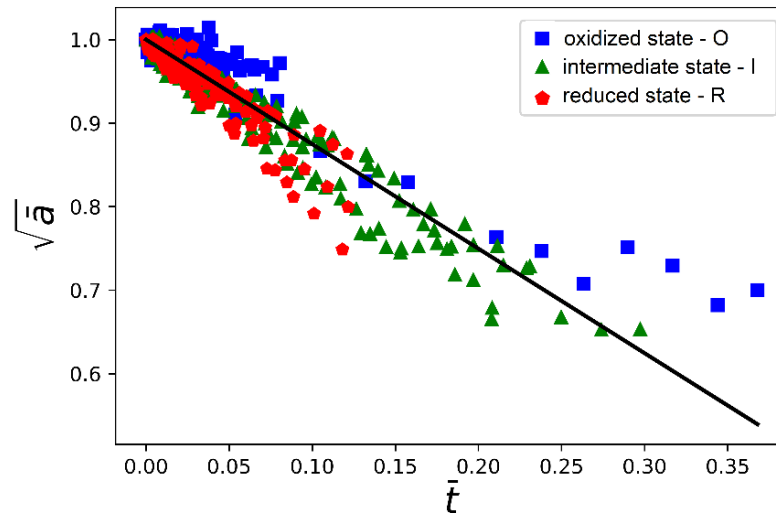


Figure 3: $\sqrt{\bar{a}}$, as a function of $\bar{t}$, is obtained for all the experiments with the nine glass samples.

By using these approaches, [4, 5, 10] we were capable to fully predict the evolution of a single bubble in melt as a function of the external conditions as well as bubble and melt features, such as temperature, melt viscosity, melt density, bubble initial radius, bubble initial composition, and others.

## 4 CASE 2: BUBBLE POPULATION

After establishing how a single-bubble behaves in a molten glass as a function of different bubble and melt states, we expand this simplified single-bubble system to a bubble population system. In our recent study from my PhD (Pereira *et al.* 2020[6]), we studied experimentally the oxygen bubble formation in a borosilicate glass melt linked to a redox reaction of a multivalent element (Ce).

The borosilicate glass powder was melted with CeO$_2$ at different temperatures (900 – 1100 °C) and durations, totaling 27 experiments. Due to cerium reduction (Eq. 1), molecular oxygen can be formed. The quenched samples were cut in two halves and the cross-sectional area of the crucible was analyzed using a *post-mortem* optical microscope approach. To support the findings, we carried out XANES spectroscopy measurements, to determine Ce speciation, and bubble gas composition.

Figure 4 displays three examples of binarized optical microscope images of samples after thermal treatment ($T = 1000$ °C). A data analysis was applied to the binarized images and bubble features, such as bubble mean density ($\langle N_b \rangle$), bubble mean diameter ($\langle d \rangle$), and bubble surface fraction ($\phi_b$) could be obtained.
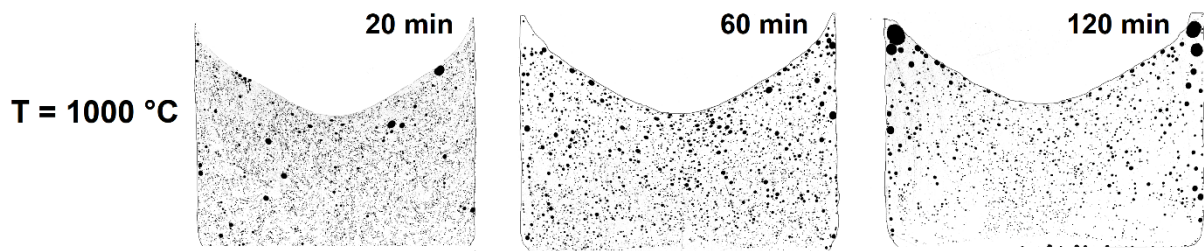
Figure 4: Binarized optical microscope images of samples treated after 1000 °C during 20, 60, and 120 min

The population of bubbles in this studied case was initially formed by air entrapment. Different experimental evidences presented in our previous work (Pereira et al. 2020 [6]) support this idea. First, both the borosilicate glass powder and the formed micro-bubbles are log-normal distributed. Second, at low temperature ($T = 800$ °C) the borosilicate glass powder packing factor and the initial bubble fraction is roughly the same (0.50). Finally, bubble gas composition results revealed that the initial composition (20 min) at 900 °C is mainly air. This type of bubble formation from pre-existing bubbles has been already recognized in the literature for non-silicate systems. It may require no energy barrier for nucleation depending on the initial size of the pre-existing bubbles.

Figure 5 shows how bubble surface fraction ($\phi_b$) in a cross-section area of the samples evolves for the five different temperatures. At the beginning, for most of the temperatures (900 to 1050°C) an increase of $\phi_b$ is noticed. After some time, this feature reaches a maximum value and it drops afterward. We believe that sample studied at 1100 °C, the mentioned initial increment takes place before 20 min of experiment. Thus, Figure 5 displays just the second part after the inflection point for this highest temperature samples.
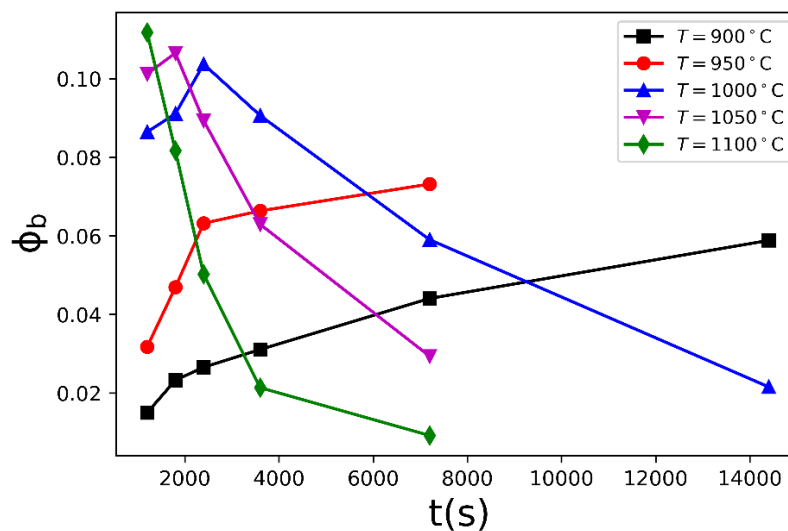


Figure 5: Bubble surface fraction ($\phi_b$) in a cross section as a function of time in the studied glass melt doped with Ce for different temperatures.

By analyzing the bubble features obtained after the data analysis of the binarized optical microscopic images, a characteristic residence time ($t_\eta$) of a bubble in a melt was proposed. It has been determined by considering the height of the glass bath (H = 20 mm), divided by $g d_{max}^2 / \eta$. This latter term comes from the Hadamard–Rybczynski solution in which the terminal rising speed of a bubble in a creeping flow (Re << 1) is obtained by a balance of the

buoyant and viscous forces balance.[11, 12] Therefore, our proposed characteristic residence time is defined as follows:

$$t_\eta = \frac{\eta H}{\rho g d_{max}^2},$$ (5)

where $\eta, \rho, g, d_{max}^2$ are respectively the melt viscosity, melt density, gravity acceleration, and the maximum bubble diameter at a given temperature. A normalization of the experimental data using this mentioned residence characteristic time was performed. First, the bubble surface fraction ($\phi_b$) is divided by the maximum surface fraction ($max\phi_b$) and the experimental time is divided by the proposed residence characteristic time (Figure 6).
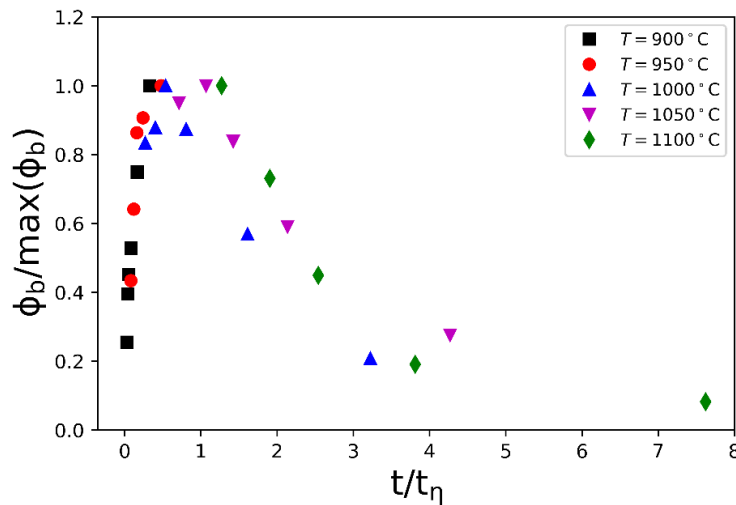


Figure 6: Normalized bubble surface fraction as a function of the normalized experimental time for the five investigated temperatures.

The other bubble features ($\langle N_b \rangle, \langle d \rangle$) were also normalized using $t_\eta$. Not only for bubble surface fraction but also for the other bubble features, a universal behavior was observed in the normalized plots. Therefore, it is really important to recognize that for all the investigated temperatures, the mechanisms governing bubble evolution are essentially the same, regardless of temperature.

The aforementioned behavior presented in Figure 5 and Figure 6 was obtained by *post-mortem* optical microscopy technique. We also obtained the same behavior in terms of bubble fraction using other different methods. In one work developed during my PhD (Pereira *et al.* 2021[13]), we proposed a novel method to infer bubble volume fraction. We applied *in-situ* impedance spectroscopy to measure the electrical resistance of a bubble-bearing melt. From the obtained electrical resistance, a conversion based on Maxwell-Wagner theory was done and the bubble volume fraction was inferred. In this same study, we validated this novel method with some well-established ones from the literature (optical microscope, low-temperature impedance spectroscopy, and apparent density).

## 5    CONCLUSION

In this work we present results of oxygen bubble formation in glass melts in the context of nuclear waste vitrification. Firstly, physico-chemical characterizations on a simplified nuclear waste glass/melt were performed. We investigated the interaction of an oxygen single-bubble and the studied borosilicate melt. By using lab-scale experiments and numerical

simulations, we were able to predict the evolution of a single bubble in melt as a function of the bubble and the melt features (melt viscosity, melt density, bubble radius, bubble initial composition, and others). We note that the mass transfer between an oxygen bubble and the cerium-bearing borosilicate liquid is significantly enhanced for both higher multivalent contents and more reduced conditions. Secondly, a population of bubbles in the simplified nuclear waste glass melt was investigated. In this latter system, insights on bubble formation by air trapping were obtained thanks to bubble imaging analyses on quenched glass samples. We proposed a characteristic residence time of bubbles in the system and by normalizing the experimental data, and a universal bubble behavior was obtained for all studied temperatures. These results indicate that the mechanisms dictating bubble behavior are independent of temperature. The results presented here have yielded a fundamental understanding of the formation of bubbles in a glass melt relevant to  nuclear waste vitrification, enabling the application of this knowledge to more complex systems in both industrial and natural contexts.

## ACKNOWLEDGMENTS

## REFERENCES

[1] C.G. Sombret, The vitrification of high-level wastes in France from the lab to industrial plants, Safety of the nuclear fuel cycle, Brussels, 1993.
[2] J. Plodinec, Glass Technology - European Journal of Glass Science and Technology Part A 41 (2000) 186-192.
[3] O. Pinet, I. Hugon, S. Mure, Procedia Materials Science 7 (2014) 124-130.
[4] L. Pereira, Mechanisms of oxygen bubble formation in a glass melt in the nuclear waste vitrification context, vol PhD, PSL University - MINES ParisTech, Paris, France, 2020.
[5] L. Pereira, J. Kloužek, M. Vernerová, A. Laplace, F. Pigeonneau, Journal of the American Ceramic Society 103 (2020) 6736-6745.
[6] L. Pereira, O. Podda, B. Fayard, A. Laplace, F. Pigeonneau, Journal of the American Ceramic Society 103 (2020) 2453-2462.
[7] J. Žlutický, L. Němec, Glastech Ber. 50 (1977) 57-61.
[8] F. Pigeonneau, Chemical Engineering Science 64 (2009) 3120-3129.
[9] F. Pigeonneau, International Journal of Heat and Mass Transfer 54 (2011) 1448-1455.
[10] F. Pigeonneau, L. Pereira, A. Laplace, Chemical Engineering Science 232 (2021) 116382.
[11] J.S. Hadamard, C. R. Acad. Sci. 152 (1911) 1735–1738.
[12] W. Rybczynski, Bull. Acad. Sci. Cracovie A (1911) 40-46.
[13] L. Pereira, M. Neyret, A. Laplace, F. Pigeonneau, R. Nuernberg, International Journal of Applied Glass Science 12 (2021) 358-366.